JOURNAL OF THERMOPHYSICS AND HEAT TRANSFER
Vol. 7, No. 4, Oct.–Dec. 1993

Radiation and Phase Change of Lithium Fluoride in an Annulus

Kurt O. Lund*
University of California, San Diego, La Jolla, California 92093

A one-dimensional thermal model is developed to evaluate the effect of radiation on the phase change of lithium-fluoride (LiF) in an annular canister under gravitational and microgravitational conditions. Specified heat flux at the outer wall of the canister models focused solar flux; adiabatic and convective conditions are considered for the inner wall. A two-band radiation model is used for the combined-mode heat transfer within the canister, and LiF optical properties relate metal surface properties in vacuum to those in LiF. For axial gravitational conditions, the liquid LiF remains in contact with the two bounding walls, whereas a void gap is used at the outer wall to model possible microgravitational conditions. For the adiabatic cases, exact integrals are obtained for the time required for complete melting of the LiF. Melting was found to occur primarily from the outer wall in the 1-*g* model, whereas it occurred primarily from the inner wall in the μ-*g* model. For the convective cases, partially melted steady-state conditions and fully melted conditions are determined to depend on the source flux level, with radiation extending the melting times.

Nomenclature

A = adiabatic wall 2, area m^2
B = Biot-type (convective) wall 2
C = liquid contact at wall 1
c = specific heat, J/kg K
f = radiation function, Appendix A
G = void gap at wall 1
g_s = scaled heat flux source, g_{sm}/ε_{0m}
g_{sm} = scaled heat flux source, $q_s/\sigma T_m^4$
H = heat of fusion, J/kg
h = heat transfer coefficient, W/m^2 K
I = radiation integral, Appendix A
K = scaled linearized radiation conductance
k = conductivity, W/m K
N = radiation/conduction number, $\varepsilon_{0m}N_m$
N' = radiation/conduction number, NK_a
N_m = radiation/conduction number, $\sigma T_m^3 \Delta r/k_{el}$
P = radiation exchange function, Appendix A
Q = rate of heat transfer, W
q_s = heat flux source, W/m^2
R = thermal resistance; K/W, K^4/W
r = radius, m
Δr = phase change material overall thickness, $r_j - r_2$
T = absolute temperature, K
t = time, s
t_c = time constant; s, $\rho_l H_{sl} \Delta r^2/k_{el} T_m$
u, v = logarithmic functions
w = width (thickness) of wall, m
α = wall energy storage ratio, $w_1 \rho_w c_w T_m/\Delta r \rho_l H_{sl}$
β = Biot number, $h_2 \Delta r/k_{el}$
Γ = radius ratio, r_2/r_j
δ_j = outer scaled liquid thickness, $(r_j - r_{jm})/\Delta r$
δ_2 = inner scaled liquid thickness, $(r_{2m} - r_2)/\Delta r$
ε = emissivity
θ = scaled temperature defect, $(\psi - 1)/Ng_s$
κ = conductivity ratio, k_{es}/k_{el}
Λ = $1 - \Gamma$, $\Delta r/r_1$
μ = radiation parameter, ≈ 0.163
ρ = density, kg/m^3
σ = Stefan-Boltzmann constant, 5.67×10^{-8} W/m^2 K^4
τ = scaled time, t/t_c
τ' = scaled time for adiabatic wall 2, $Ng_s\tau = tq_s/\rho_l H_{sl} \Delta r$
τ'' = scaled time for convective wall 2, $(1 - \psi_f)\tau = tk_l(T_m - T_f)/\rho_l H_{sl} \Delta r^2$
ϕ = flux index
ψ = temperature ratio, T/Tm

Subscripts

a = a band (transparent band) of spectrum
b = b band (optically thick band)
e = effective
f = fluid boundary
fm = fully melted
h = convective
i = surface index, j or 2
j = surface index, 1 or 3
k = conduction
l = liquid
m = melting condition or temperature
r = radiative
s = solid, source
st = storage
w = wall
0 = vacuum, initial conditions
1 = wall 1, outer wall
2 = wall 2, inner wall
3 = surface 3 (at gap facing outer wall)

Received March 1, 1991; revision received Dec. 16, 1991; accepted for publication Oct. 14, 1992.

*Assistant Research Engineer, Center for Energy and Combustion Research. Member AIAA.

Introduction

THE behavior of phase transition is central to the understanding of phase-change thermal energy storage for development of solar dynamic space power.[1] Therefore, ground tests have been conducted,[2] Space Shuttle flight experiments have been planned,[3,4] and numerical analyses have been performed to determine two-dimensional[5] and three-dimensional[6] effects of the phase transition process. These analyses and experiments utilize an annular canister containing the phase change material (PCM), where a solar heat flux (or electrically simulated flux) is impressed on the outer wall of the canister (r_1 in Fig. 1); the inner wall (r_2) either is convective or is nearly adiabatic during the heat addition.

In application to heat receivers, the PCMs are high-temperature salts, such as lithium-fluoride (LiF) with a melting

temperature of 1120 K (1556°F) [or the eutectic LiF-CaF_2 which melts at 1040 K (1412°F)]. At these temperatures radiative transport can be a significant part of the overall heat transfer processes within the canisters. In the previous two-dimensional model[5] radiation was not included, and in the three-dimensional model[6] the effect of radiation is obscured by the complexity of the numerical computations; in the flight experiments,[3,4] radiation will occur naturally, but the radiative effect cannot be determined directly and must be deduced from canister surface temperatures. Therefore, there is a need for basic models and solutions for the high-temperature enclosure with PCM and radiation; a one-dimensional analysis is presented in this article.

The high-temperature salts exhibit considerable contraction upon solidification, which can lead to void formation at the outer wall under microgravity conditions in space. Hence, in this case, radiation is the dominant mode of heat transfer, in contrast to axial 1-g conditions where liquid PCM contacts the wall and conduction is dominant. Four cases are considered here which model behaviors for adiabatic and convective inner wall conditions, and under axial 1-g and μ-g conditions.

Radiation within the canister enclosure follows conventional spectral exchange between surfaces, except that the intervening medium, LiF, has spectral properties which differ from those of vacuum. Therefore, accurate application requires spectral integrations; these are presented in Appendix A where metal surface properties in vacuum are related to those in the presence of the LiF medium. Following Williams[7] and Song and Viskanta,[8] a two-band approximation is made utilizing recent measurements of LiF optical properties as summarized by Palik and Hunter.[9]

A two-surface thermal model is developed in the next section for adiabatic and convective boundary conditions at the inner radius, and imposed heat flux at the outer radius. This differs from the usual Stefan problem where the temperature at a boundary is suddenly changed (e.g., Yao and Prusa,[10] Burmeister,[11] or Solomon[12]), resulting in a boundary layer growing in time as the error function (e.g., Arpaci and Larsen[13]). However, as shown in Appendix B, with the presently imposed heat flux boundary condition, this layer does not develop, with the result that PCM temperatures change only slowly in a quasisteady fashion, as was previously observed.[8]

For the liquid PCM it is assumed that the conduction limit applies, such that natural convection boundary layers do not develop significantly, and such that the phase-change boundary remains axially uniform. This is valid for Rayleigh numbers below 1700 for rectangular enclosures,[14] but has also been demonstrated experimentally for much larger Rayleigh numbers with a heat flux boundary and a 4.5 aspect ratio.[15] This is considered an excellent approximation under 1-g axial gravitational acceleration; under microgravity conditions the magnitude of natural convection is suppressed, although some convection effects can be present.[16,17]

Problem Formulation

The thermal model is for a solid region surrounded by liquid at either or both r_{3m} and r_{2m}, as indicated in Fig. 1, and (in some cases) having a narrow void gap near r_1. The gap models microgravity conditions where the PCM could completely solidify, radially outwards, without making contact with the outer wall. Under axial 1-g conditions, there will be contact with the wall by liquid filling the annular gap. In these annular liquid gaps, convection will be driven by the gravitational and temperature fields, but without feedback to the thermal process for small Rayleigh numbers and long aspect annuli.[17] In the following, four cases of analysis are considered: "A" and "B" referring respectively to adiabatic and convective boundary conditions at wall 2, and "C" and "G" referring to contact and gap conditions at wall 1, respectively.

The heat transfer processes shown in Fig. 1 constitute a combined radiation and conduction network. Radiation occurs between walls 1 and 2 in the transparent spectral band of the PCM (the a band), and to a lesser extent between surfaces 1 and 3 in the optically thick band of the spectrum (the b band), as shown in Appendix A. In each case considered, the initial condition is fully solidified PCM at wall 1 (or surface 3), and at the melting temperature T_m. Under this condition the sensible heat terms do not enter the problem, and the quasisteady network indicated in Fig. 1 provides the whole solution, as shown in Appendix B.

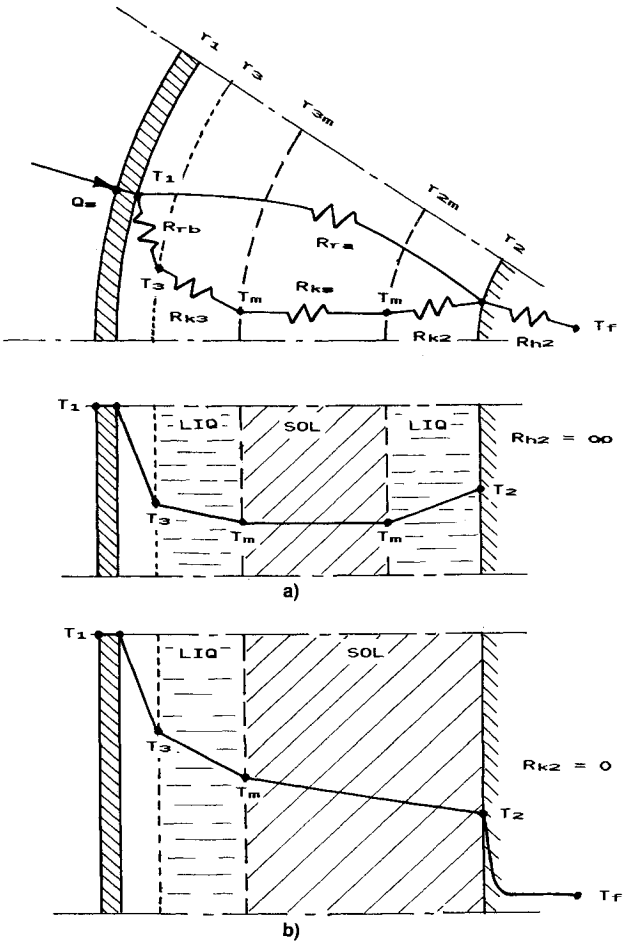

Fig. 1 Thermal model for radiation and phase-change in an annulus: a) adiabatic inner wall, b) convective inner wall.

With reference to Fig. 1, the conduction heat transfer from surface i to im ($i = j$ or 2, $j = 1$ or 3) is given by

$$Q_{ki} = (T_i - T_{im})/R_{ki} \tag{1}$$

where resistances are

$$R_{kj} = \frac{\ell_n (r_j/r_{jm})}{2\pi k_{el}}, \qquad j = 1, 3 \tag{2}$$

$$R_{k2} = \frac{\ell_n (r_{2m}/r_2)}{2\pi k_{el}} \tag{3}$$

Similarly

$$Q_{ks} = \frac{T_{jm} - T_{2m}}{R_{ks}} \tag{4}$$

$$R_{ks} = \frac{\ell_n (r_{jm}/r_{2m})}{2\pi k_{es}}, \qquad j = 1, 3 \tag{5}$$

$$Q_{h2} = h_2 A_2 (T_2 - T_f) \tag{6}$$

$$Q_{st1} = (\rho c)_w A_1 w_1 \frac{dT_1}{dt} \tag{7}$$

Energy balances yield, respectively, on surface 1

$$Q_s = Q_{ra} + \begin{cases} Q_{k1}; & C \\ Q_{rb} + Q_{st1}; & G \end{cases} \tag{8}$$

on surface 2

$$Q_{ra} = \begin{cases} Q_{k2}; & A \\ Q_{h2} - Q_{ks}; & B \end{cases} \tag{9}$$

and on surface 3

$$Q_{rb} = Q_{k3} \tag{10}$$

The radiative heat rates are related to temperatures as

$$Q_{ra} = 2\pi r_1 \varepsilon_{0m} \sigma T_m^4 P_a(\psi_1, \psi_2) \tag{11}$$

$$Q_{rb} = 2\pi r_1 \varepsilon_{0m} \sigma T_m^4 \mu P_b(\psi_1, \psi_3) \tag{12}$$

where, from Appendix A

$$P_a = \psi_1^{4.5} I_1(\psi_1, \psi_2) - \psi_2^{4.5} I_2(\psi_1, \psi_2) \tag{13}$$

$$P_b = \psi_1^4 - \psi_3^4 \tag{14}$$

and $\mu \approx 0.163$ is a small parameter.

At the phase boundaries the heat added results in the movement of the boundaries through H_{sl}, the latent heat

$$Q_{kj} - Q_{ks} = -2\pi \rho_l H_{sl} r_{jm} \frac{dr_{jm}}{dt}, \qquad j = 1, 3 \tag{15}$$

$$Q_{k2} + Q_{ks} = +2\pi \rho_l H_{sl} r_{2m} \frac{dr_{2m}}{dt} \tag{16}$$

In scaled, nondimensional terms, the above relations are combined and summarized as follows:

Wall 1

$$Ng_s = NP_a + \begin{cases} (\psi_1 - 1)/v_1, & C \\ \mu NP_b + \alpha \, d\psi_1/d\tau, & G \end{cases} \tag{17}$$

Wall 2

$$\frac{\psi_2 - 1}{u_j} + \beta\Gamma(\psi_2 - \psi_f) = NP_a \tag{18}$$

$$u_j = \begin{cases} \ell n \, (1 + \Lambda\delta_2/\Gamma)/\Lambda, & A \\ \ell n \, [(1 - \Lambda\delta_j)/\Gamma]/\kappa\Lambda, & B \end{cases} \tag{19}$$

Surface jm (j = 1 or 3)

$$(1 - \Lambda\delta_j) \frac{d\delta_j}{d\tau} = \frac{\psi_j - 1}{v_j} - \begin{cases} 0, & A \\ (1 - \psi_2)/u_j, & B \end{cases} \tag{20}$$

$$v_j = \ell n \, [1/(1 - \Lambda\delta_j)]/\Lambda \tag{21}$$

Surface 2m

$$(\Gamma + \Lambda\delta_2) \frac{d\delta_2}{d\tau} = NP_a, \quad A \tag{22}$$

Surface 3

$$[(\psi_3 - 1)/v_3] = \mu NP_b, \quad G \tag{23}$$

Results

Case *C-A*

Under axial 1-g conditions with liquid contacting wall 1 (C cases), the energy storage in the canister walls is negligible and the impressed heat flux effectively acts directly on the PCM. With an adiabatic wall 2, conservation of energy requires all of the energy to go into phase change; this results in a closed form solution of the system [Eqs. (17–23)], obtained from the sum of Eqs. (20) and (23):

$$\delta_1 - \Lambda\delta_1^2/2 + \Gamma\delta_2 + \Lambda\delta_2^2/2 = Ng_s\tau \equiv \tau' \tag{24}$$

In particular, for complete melting when $r_{2m} = r_{1m}$ ($\delta_1 + \delta_2 = 1$), the scaled time is obtained from Eq. (24) as

$$Ng_s\tau_{fm} = \tau'_{fm} = (1 + \Gamma)/2 \tag{25}$$

or, in dimensional variables, the fully melted time is

$$t_{fm} = \frac{\pi(r_1^2 - r_2^2)\rho_l H_{sl}}{2\pi r_1 q_s} \tag{26}$$

Thus, for case C-A, the time to melt the PCM is the phase-change heat content, divided by the input heat transfer rate.

Because of the liquid contact with the canister walls, the wall temperatures do not depart strongly from T_m; therefore, for the C cases, it is adequate to use the linearized radiation exchange, $P_a(\psi_1, \psi_2) \approx K_a(\psi_1 - \psi_2)$, where the constant is $K_a \approx 4.5 f_{0c}(1)$, and f_{0c} is from Fig. A1 of Appendix A.

For the parallel plate limit ($\Lambda \to 0$, $\Gamma \to 1$) the adiabatic, linearized system has the exact solutions

$$\theta_1 = \frac{\tau'}{2}\left(\frac{2 + N'\tau'}{1 + N'\tau'}\right) \tag{27}$$

$$\theta_2 = \frac{\tau'}{2}\left(\frac{N'\tau'}{1 + N'\tau'}\right) \tag{28}$$

$$\delta_1 = \frac{\tau'}{4}\left(\frac{2 + N'\tau'}{1 + N'\tau'}\right)\frac{1 + (1 + N'\tau')^2}{(1 + N'\tau')^2} \tag{29}$$

$$\delta_2 = \frac{\tau'}{2}\left(\frac{2 + N'\tau'}{1 + N'\tau'}\right)\left(\frac{N'\tau'}{1 + N'\tau'}\right)^2 \tag{30}$$

These solutions clearly show the double surface phase-change phenomenon (as also indicated in Fig. 1a). It is seen in Eqs. (29) and (30) that δ_1 grows linearly with τ' for small $N'\tau'$ (i.e., initially), whereas δ_2 grows quadratically; the initially linear phase boundary growth has been observed previously in the absence of radiation.[18]

Wall temperatures are determined in this analysis, rather than specified. The gradual increase in the wall temperatures in Eqs. (27) and (28) shows the absence of thermal boundary layers, as proved in Appendix B. From Eq. (27), the maximum wall temperature increase at complete melting when $\tau' = 1$ is $\psi_{1,max} - 1 = Ng_s$; in physical terms $T_{1,max} - T_m = q_s(r_1 - r_2)/k_{el}$, or about 25 K above 1120 K, which validates linearization of the radiation term.

In the case of an annulus with finite radii ($r_2/r_1 = \Gamma \neq 1$), Eqs. (17–22) were solved by numerical integration, with results as shown in Fig. 2, for $\Gamma = 0.5$. The initially linear and quadratic growth of the two phase fronts is evident; complete melting occurred at $\tau'_{fm} = 0.75$, as predicted by Eq. (25).

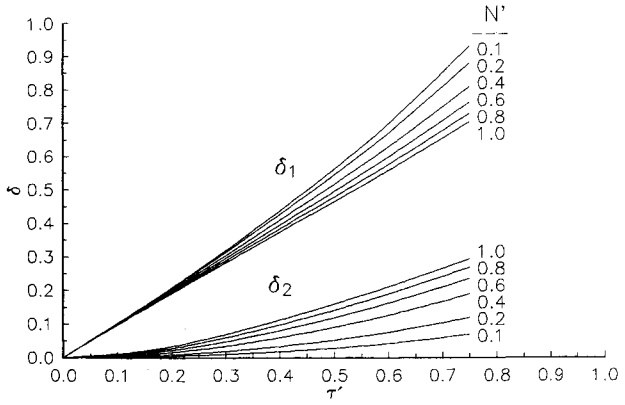

Fig. 2 Growth of phase-change fronts for annulus with $\Gamma = 0.5$ (liquid contacts outer wall, adiabatic inner wall).

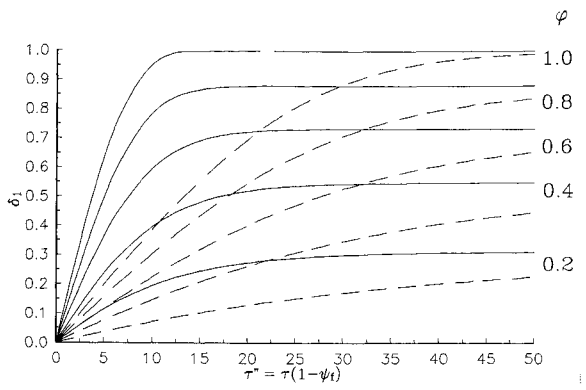

Fig. 3 Steady-state, partially melted phase fronts in annulus with $\Gamma = 0.5$ (liquid contacts outer wall; convective inner wall; $N' = 0.2$; $\kappa = 1.5$; ——, $\beta = 1$; -----, $\beta = 0.5$).

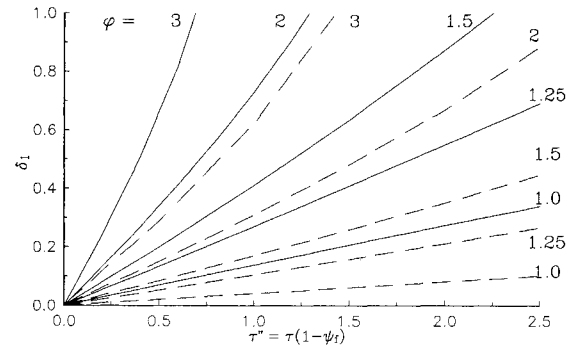

Fig. 4 Fully-melted phase fronts in annulus with $\Gamma = 0.5$ (liquid contacts outer wall; convective inner wall; $N' = 0.2$; $\kappa = 1.5$; ——, $\beta = 1$; -----, $\beta = 0.5$).

Case *C-B*

With the convection heat sink at the inner wall, the possibility exists that q_s may not be sufficient to cause any melting at all. This is seen from the combination of Eqs. (17–20) which yields

$$(1 - \Lambda\delta_1)\frac{d\delta_1}{d\tau} = Ng_s - \beta\Gamma(\psi_2 - \psi_f) \tag{31}$$

where the initial slope must be positive for δ_1 to grow; thus, Ng_s must be greater than the minimum

$$Ng_{s0} = \beta\Gamma(\psi_{20} - \psi_f) = \beta\Gamma\frac{N' + 1/u_0}{N' + 1/u_0 + \beta\Gamma}(1 - \psi_f) \tag{32}$$

where from Eq. (19) $u_0 = \ln(1/\Gamma)/\kappa\Lambda$, and $\psi_{20} = \psi_2(0)$ is obtained from Eq. (18). In dimensional variables with $h_{r1} = \varepsilon_{0m}\sigma T_m^3 K_a$, the limiting minimum heat flux for phase change to occur is

$$q_{s0} = \frac{T_m - T_f}{(r_1/h_2r_2) + \{r_1/[h_{r1}r_1 + k_{es}/\ln(r_1/r_2)]\}} \tag{33}$$

which is the initial overall temperature difference over the total thermal resistance. Similarly, there is a critical heat flux for which the PCM just becomes 100% melted, and at steady state with zero slope at $\delta_1 = 1$; this is given by Eq. (31) as

$$Ng_{s1} = \beta\Gamma(1 - \psi_f) \tag{34}$$

or

$$q_{s1} = h_2(T_m - T_f)r_2/r_1 \tag{35}$$

Partially melted and unmelted, conditions have also been observed experimentally.[2] Finally, there is a limiting flux above which melting occurs from both sides

$$Ng_{s2} = Ng_{s1}\left(1 + \left\{\frac{1}{(N'/\kappa\Lambda)\ln[1/(1 - \Lambda)]}\right\}\right) \tag{36}$$

however, for small N', this is a high flux which is usually not encountered.

To summarize, $g_s < g_{s0}$ results in no phase change, $g_{s0} \le g_s < g_{s1}$ results in a steady state with only partial melting, $g_{s1} \le g_s < g_{s2}$ results in 100% melting in finite time from wall 1, and $g_s \ge g_{s2}$ results in 100% melting in finite time from both walls.

The numerical integration of the system equations for the partially melted case is shown in Fig. 3, where the scaled heat flux was taken as

$$g_s = \phi g_{s1} + (1 - \phi)g_{s0}, \qquad 0 \le \phi \le 1 \tag{37}$$

For the parallel plate limit, the partially melted steady-state condition can be obtained analytically as

$$\delta_{1,ss} = \phi\frac{N' + \kappa + \beta}{N' + \kappa + \phi\beta + (1 - \phi)(\kappa - 1)N'} \tag{38}$$

For $g_s > g_{s1}$, the phase-change front grows rapidly to complete melting, as shown in Fig. 4, where the applied flux was taken as $g_s = \phi g_{s1} < g_{s2}$.

Case *G-A*

Under microgravity conditions where a void gap may form between the PCM and the outer wall (G cases), there is *only* radiative transport between the outer wall and the PCM. This will cause considerable temperature increase in wall 1, and some energy storage in the wall.

There are no further simplifications possible to the system [Eqs. (17–23)]. Nevertheless, for an adiabatic wall 2, it possesses the exact integral

$$\alpha(\psi_1 - 1) + \delta_3 - \Lambda\delta_3^2/2 + \Gamma\delta_2 + \Lambda\delta_2^2/2 = Ng_s\tau \equiv \tau' \tag{39}$$

which, for the fully melted condition, $\delta_2 + \delta_3 = 1$, reduces to

$$\tau'_{fm} = (1 + \Gamma)/2 + \alpha(\psi_{1,fm} - 1) \tag{40}$$

By comparison with Eqs. (24) and (25), these results represent the sum of the energies stored in the PCM and in wall 1. Exact calculation of the melting time from Eq. (40) is not

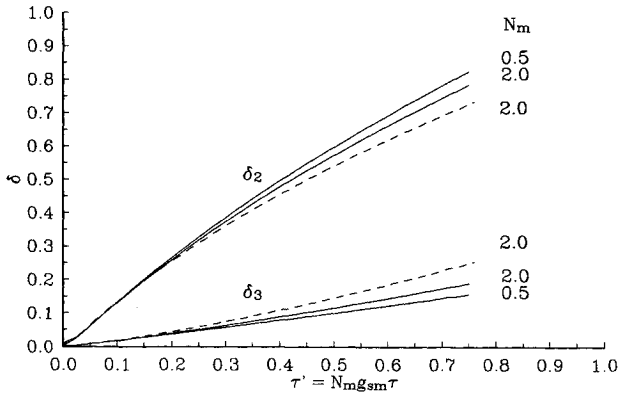

Fig. 5 Growth of phase-change fronts for annulus with $\Gamma = 0.5$ (gap at outer wall; adiabatic inner wall; $g_{sm} = 0.1$; $\alpha = 0.1$; ——, $\varepsilon_{0m} = 0.1$; -----, $\varepsilon_{0m} = 0.3$).

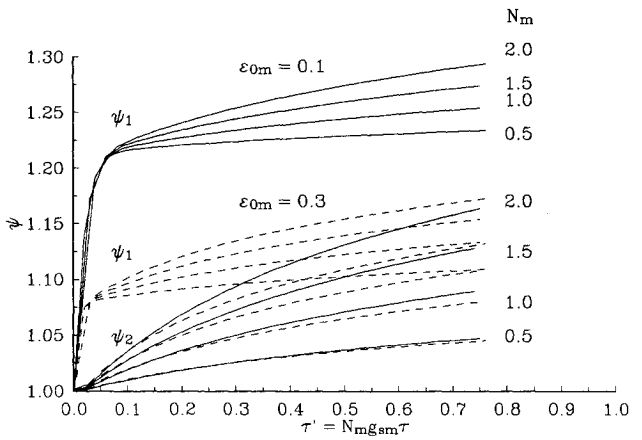

Fig. 6 Wall temperatures for annulus with $\Gamma = 0.5$ (gap at outer wall; adiabatic inner wall; $g_{sm} = 0.1$; $\alpha = 0.1$).

immediate, because the original system must be solved to determine wall temperature ψ_1 at any time; however, the ratio of wall capacitance to phase-change capacitance is a small quantity, $\alpha = \mathbb{O}(0.1)$, so that melting times are only slightly longer than for liquid contacting wall 1.

A numerical integration of system [Eqs. 17–23)] for $\Gamma = 0.5$, $g_{sm} = 0.1$, $\alpha = 0.1$, and for radiation functions from Fig. A1, is shown in Fig. 5. In contrast to case *C-A*, most of the melting takes place from the inner wall, and only a slight amount near the outer wall; otherwise, the melting is completed in about the same time as previously, because of the small value of α.

The corresponding wall temperature variations are shown in Fig. 6, where there is a dramatic sudden increase in the outer wall temperature, in contrast to the liquid contact case where this temperature increased only slightly and gradually. Asymptotic analysis shows this initial temperature "jump" to be approximated by

$$\psi_{1,\text{outer}}(0) = [1 + g_{sm}/\varepsilon_{0m} f_{0g}(1)]^{1/4.5} \qquad (41)$$

The effect of the emissivity on ψ_1 is evident in both Eq. (41) and Fig. 6, whereas there is a smaller effect on ψ_2; the interface temperature ψ_3 increased only slightly from 1. Clearly from Eq. (41), an increase in the applied flux g_{sm} would cause a further increase in the outer wall temperature.

Case *G-B*

With the gap at the outer wall, and convection at the inner wall, the flux limit definitions for g_{s0} [Eq. (32)] and g_{s1} [Eq. (34)] apply as previously; however, ψ_2 must now be calculated from the nonlinear equations. Because μ is a small quantity, it is found for the steady-state limit that $\psi_{20} = 1 - \mathbb{O}(\mu N)$,

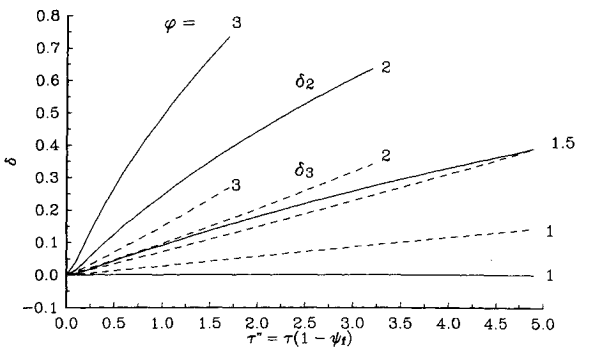

Fig. 7 Growth of phase-change fronts for annulus with $\Gamma = 0.5$ (gap at outer wall; convective inner wall; $\alpha = 0.1$; $\varepsilon_{0m} = 0.1$; $\beta = 0.5$; $N_m = 1$; $\psi_f = 0.8$; $\kappa = 1.5$).

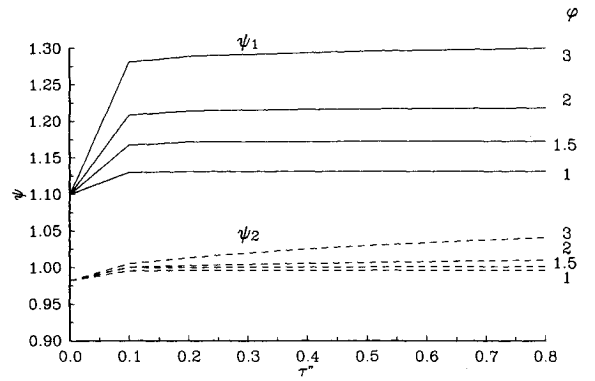

Fig. 8 Wall temperatures for annulus with $\Gamma = 0.5$ (gap at outer wall; convective inner wall; $\alpha = 0.1$; $\varepsilon_{0m} = 0.1$; $\beta = 0.5$; $N_m = 1$; $\psi_f = 0.8$; $\kappa = 1.5$).

such that $g_{s0} = g_{s1}[1 - \mathbb{O}(\mu)]$; that is, for any phase change to occur at all, g_s must be very near the limit, g_{s1}. Above this limit, $g_{s2} = g_{s1}[1 + \mathbb{O}(\mu)]$, so that melting will occur from wall 2 for g_s just slightly above g_{s1}.

An example of this behavior is shown in Fig. 7, where $g_s = \phi g_{s1}$: for $\phi = 1$ there is only slight melting from surface 3, and no melting at surface 2; for $\phi = 1.5$ the melting rates are about the same from both surfaces, but a long time is required for complete melting; for $\phi \geq 2$ the melting rate is greater from surface 2, the inner wall, and complete melting was attained for the times τ'' shown in the figure. Comparison with the adiabatic cases in Fig. 4 shows that a longer melting time is needed with convective heat transfer, as expected.

Corresponding temperatures are shown in Fig. 8: after the initial jump, these remain essentially constant during the melting process. With the initial condition of $\delta_3(0) = 0$ [$\psi_3(0) = 1$], $\psi_1(0)$ is greater than 1, approximately as given by Eq. (41), and $\psi_2(0)$ is slightly less than 1, as shown.

Conclusions

Four analytical cases have been considered for the melting of lithium-fluoride in an annulus with impressed heat flux at one boundary, including the effect of internal radiation heat transfer. It was found that this process is quasisteady when the solid LiF near the outer wall is initially at the melting temperature. Radiation was found to be an important effect, especially in the presence of void gaps near the outer wall.

For the adiabatic inner wall condition, the time for complete melting is a fixed quantity which depends only slightly on voids. However, the location of the phase boundaries is strongly influenced by the void gap, with melting occurring primarily from the outer wall when there is liquid contact, and primarily from the inner wall when there is a void gap at wall 1. Wall temperatures remained close to the melting temperature with liquid PCM contacting wall 1; but, the wall-1 temperature has a large and sudden increase above the melting temperature when a void gap is present at wall 1.

For the convective inner wall conditions there may or may not be complete melting, depending on the level of impressed heat flux, relative to the fluid temperature and other problem parameters. For liquid PCM contacting wall 1, melting occurred only from wall 1 for moderate heat fluxes, and steady-state partially melted conditions were determined; for a void gap at wall 1, conditions for partial melting almost did not exist and a substantially high heat flux is required in order to cause any melting at all.

In summary, the results show fundamentally different behaviors, depending on the boundary conditions employed. Thus, experimental results from the flight experiments, where the inner wall is essentially adiabatic, cannot be used directly for convection applications, without interpretive analytical/numerical modeling; nor can ground-based results, under 1-g acceleration, be used directly in microgravity applications.

Appendix A: Radiation Model

Experimental data for LiF[9] indicate a near-perfect transparency for wavelengths below 5.5 μm, and optically thick properties for wavelengths above about 7 μm. Therefore, a two-band radiation model is considered where the LiF is transparent for wavelengths below 5.5 μm (the a band), and optically thick for wavelengths above this value (the b band). (This model obviously neglects processes in a narrow band where the LiF is neither transparent nor optically thick.)

In the a band there is radiation exchange between the two bounding metal walls, and spectral variations of properties of the walls, and of the LiF with index of refraction n are included. In the vicinity of $T_m = 1120$ K, most of the emitted radiation is in this transparent band. In the b band, there is a minor radiative addition to the LiF conductivity and, in the presence of a void, minor radiation between wall 1 and the LiF surface.

Wall Emissivity

Spectral emission into a medium with refractive index n is given by the Planck formula and the spectral emissivity[19]

$$e_\nu = \varepsilon_\nu e_{b\nu} = n^2 \varepsilon_\nu e_{b\zeta} \equiv \varepsilon_\zeta e_{b\zeta} \tag{A1}$$

where $\zeta = c_2/n\lambda T = \nu/\nu_0$, $\nu_0 = c_0 T/c_2$, $c_0 = 3 \times 10^8$ m/s, $c_2 = 14{,}388$ μm K, and where

$$e_{b\zeta} = \frac{15}{\pi^4} \frac{\sigma T^4}{\nu_0} \frac{\zeta^3}{e^\zeta - 1} \tag{A2}$$

Here, ε_ν represents emission into the medium relative to blackbody emission into the medium, and ε_ζ represents emission into the *medium* relative to blackbody emission into *vacuum*; the latter can be greater than one whenever n is greater than one.

For a number of metal surfaces at the high temperatures under consideration, experiments have shown that the normal spectral emissivity varies with wavelength to the $-\frac{1}{2}$ power, even into the visible part of the spectrum[20,21]; therefore consistent with electromagnetic theory, we take

$$\varepsilon_\nu = \varepsilon_\lambda = n\varepsilon_{\lambda c}\sqrt{(\lambda_c/n\lambda)} = n\varepsilon_{\lambda c}\sqrt{(\zeta/\zeta_c)} \tag{A3}$$

where $\varepsilon_{\lambda c}$ is the best-fit emissivity for $n = 1$ at wavelength λ_c, and where $\zeta_c = c_2/\lambda_c T$. For emission into vacuum, this model yields the total normal emissivity

$$\varepsilon_{0t} = \frac{\varepsilon_{\lambda c}}{\sqrt{\zeta_c}} \frac{15}{\pi^4} \int_0^\infty \frac{\zeta^{3.5}\, d\zeta}{e^\zeta - 1} = \frac{1}{c_4} \frac{\varepsilon_{\lambda c}}{\sqrt{\zeta_c}} \tag{A4}$$

where $c_4 = \pi^4/(15 \times 12.27) = 0.529$. For example, for Nickel at 1390 K with the experimental value $\varepsilon_{\lambda c} = 0.25$ at $\lambda_c = 1$ μm (Seban[20]), the model yields $\varepsilon_{0t} = 0.147$; for $\varepsilon_{\lambda c} = 0.08$ at $\lambda_c = 9$ μm it yields $\varepsilon_{0t} = 0.141$, which indicates good agreement with experimental measurements for this material at this temperature.

Now combining Eqs. (A1), (A2), and (A4), the effective spectral emissivity for emission into medium n is given by

$$\varepsilon_\zeta = c_4 n^3 \varepsilon_{0t}\sqrt{\zeta} \tag{A5}$$

Thus, if the total normal (hemispherical) emissivity function $\varepsilon_{0t}(T/T_m)$ for emission into vacuum is known in the vicinity of T_m, then Eq. (A5) yields an approximate spectral normal (hemispherical) emissivity for emission into medium n. For example, with $\varepsilon_{0t} = 0.147$ from the above calculation, the emissivity at $\lambda = 1$ μm for emission into LiF ($n \approx 1.4$) is 0.58.

A-Band Radiation Exchange

Application of radiosity microbalance[22,23] to the phases and surfaces in Fig. 1, yields the spectral flux at wall 1

$$q_{\zeta 1} = \frac{e_{b\zeta 1} - e_{b\zeta 2}}{(1/\varepsilon_{\zeta 1}) + [(1/F_{12})/\varepsilon_{\zeta 2}] - \tau_e} \tag{A6}$$

where the effective interface transmittance is

$$\tau_e = (1 - 2\rho_3)/(1 - \rho_3) \approx \tau_3 \approx 0.98$$

Thus, the a band total radiative flux is

$$q_{a1} = \int_{\nu_a}^\infty q_{\nu 1}\, d\nu = \nu_0 \int_{\zeta_a}^\infty q_{\zeta 1}\, d\zeta \tag{A7}$$

Combining Eq. (A2) with Eqs. (A5–A7), results in

$$(q_{a1}/\varepsilon_{0m}\sigma T_m^4) = \psi_1^{4.5} I_1 - \psi_2^{4.5} I_2 \tag{A8}$$

where

$$I_i = \frac{1}{12.27} \times \int_{\zeta_{ai}}^\infty \frac{\zeta^{3.5}/(e^\zeta - 1)\, d\zeta}{[\varepsilon_{0m}\sqrt{\psi_1}/n_1^3 \varepsilon_{0t}(\psi_1)] + [\varepsilon_{0m}\sqrt{\psi_2}/F_{12} n_2^3 \varepsilon_{0t}(\psi_2)] - c_4 \varepsilon_{0m}\tau_3\sqrt{\psi_i \zeta}} \tag{A9}$$

and $\zeta_{ai} = \zeta_{am}/\psi_i$, $\zeta_{am} = c_2\nu_a/c_0 T_m$, $\psi_i = T_i/T_m$, $\varepsilon_{0m} = \varepsilon_{0t}(1)$.

In Eq. (A9), $n_1 = n(\psi_1\zeta)$ and $n_2 = n(\psi_2\zeta)$ for LiF contact with both walls, whereas $n_1 = 1$ in the presence of a void gap at wall 1; for the region considered, the LiF spectral refraction index data of Palik and Hunter[9] may be represented as a function of wave number, as follows:

$$n(\psi\zeta) = 1.38 + 7.79 \times 10^{-4}\psi\zeta - 2.3e^{-1.87\psi\zeta} \tag{A10}$$

A closed-form integration of Eq. (A9) is not possible; however, it may be evaluated in the vicinity of T_m by use of Taylor series expansions about this temperature. Since wall temperatures, on an absolute scale, do not depart strongly from T_m, this is a valid procedure, which yields for LiF contact with walls 1 and 2

$$I_{i,c} = f_{0c}(\psi_i) + \left(\psi_1 - 1 + \frac{\psi_2 - 1}{F_{12}}\right) \times \left\{\left(\frac{\varepsilon'_{0m}}{\varepsilon_{0m}} - \frac{1}{2}\right) f_{1c}[\psi_i; n(\zeta)] + f_{2c}(\psi_i)\right\} + \varepsilon_{0m}(\psi_i - 1) f_{3c}(\psi_i) \tag{A11}$$

and for a void gap at wall 1

$$I_{i,g} = f_{0g}(\psi_i) + (\psi_1 - 1)\left(\frac{\varepsilon'_{0m}}{\varepsilon_{0m}} - \frac{1}{2}\right) f_{1g}(\psi_i; 1)$$

$$+ \frac{\psi_2 - 1}{F_{12}}\left\{\left(\frac{\varepsilon'_{0m}}{\varepsilon_{0m}} - \frac{1}{2}\right) f_{1g}[\psi_i; n(\zeta)] + f_{2g}(\psi_i)\right\}$$

$$+ \varepsilon_{0m}\tau_3(\psi_i - 1) f_{3g}(\psi_i) \tag{A12}$$

where for $\gamma = c$ or g

$$f_{0\gamma}(\psi_i) = \frac{1}{12.27}\int_{\zeta_{am}/\psi_i}^{14} \frac{g(\zeta)\,d\zeta}{D_{0\gamma}} \tag{A13}$$

$$f_{1\gamma}(\psi_i; n) = \frac{1}{12.27}\int_{\zeta_{am}/\psi_i}^{14} \frac{g(\zeta)\,d\zeta}{D_{0\gamma}^2 n^3} \tag{A14}$$

$$f_{2\gamma}(\psi_i) = \frac{3}{12.27}\int_{\zeta_{am}/\psi_i}^{14} \frac{\zeta n'(\zeta) g(\zeta)\,d\zeta}{D_{0\gamma}^2 n^4(\zeta)} \tag{A15}$$

$$f_{3\gamma}(\psi_i) = \frac{c_4/2}{12.27}\int_{\zeta_{am}/\psi_i}^{14} \frac{\sqrt{\zeta} g(\zeta)\,d\zeta}{D_{0\gamma}^2} \tag{A16}$$

Here, the denominators are

$$D_{0c} = \{[(1 + 1)/F_{12}]/n^3(\zeta)\} - c_4\varepsilon_{0m}\sqrt{\zeta} \tag{A17}$$

$$D_{0g} = 1 + [1/F_{12}n^3(\zeta)] - c_4\varepsilon_{0m}\tau_3\sqrt{\zeta} \tag{A18}$$

and the numerator function is

$$g(\zeta) = [\zeta^{3.5}/(e^{\zeta} - 1)] \tag{A19}$$

which is less than 1% at the computational upper limit of $\zeta = 14$; here $'$ denotes the derivative with respect to the function argument. A sample evaluation of $f_{0\gamma}$ is shown in Fig. A1.

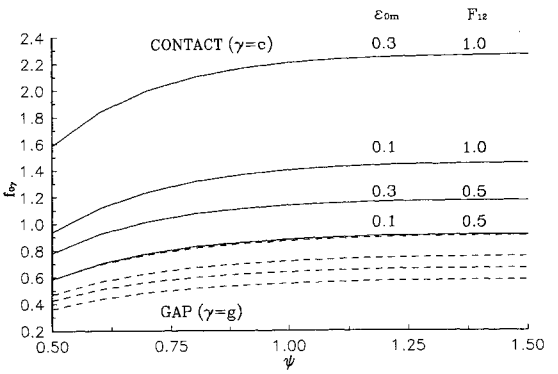

Fig. A1 Radiation function evaluation.

B-Band Radiation Effect

In the optically thick region of the spectrum there is radiation exchange across the wall-1 void gap according to

$$q_{b1} = \int_0^{\zeta_a} \frac{e_{b\zeta 1} - e_{b\zeta 3}}{(1/\varepsilon_{\zeta 1}) + (1/\varepsilon_{\zeta 3}) - 1} \tag{A20}$$

where $\varepsilon_{\zeta 1}$ is obtained as before, but with $n = 1$, and $\varepsilon_{\zeta 2}$ is obtained from electromagnetic theory as

$$\varepsilon_{\zeta 2} = \{4n/[(n + 1)^2 + k^2]\} \tag{A21}$$

With the data of Palik and Hunter,[9] evaluation of Eqs. (A20) and (A21) results in

$$q_{b1} = \mu\varepsilon_{0m}\sigma T_m^4(\psi_1^4 - \psi_3^4) \tag{A22}$$

where μ is a slightly decreasing function of increasing temperature, with an average value of $\mu = 0.163$. Thus, radiation exchange across the gap is quite small.

Energy absorption in the medium is modeled as Rosseland conductivity[22,23]

$$k_R = \int_{\lambda_a}^{\infty} \frac{4}{3a_\lambda}\frac{\partial e_{b\lambda}}{\partial T}\,d\lambda = \frac{5}{\pi^4}\sigma T^3 \int_0^{\zeta_a} \frac{\zeta^4 e^{\zeta}}{a_\lambda(e^{\zeta} - 1)^2}\,d\zeta \tag{A23}$$

where $a_\lambda = 4\pi k/\lambda$. Evaluation of this function shows but a weak temperature dependence, and an approximate value of 0.005 W/cm K, which is an order of magnitude less than the medium thermal conductivity. Thus, there is only minor b-band radiative effect on the phase-change heat transfer problem.

Appendix B: Asymptotic Analysis of the Flux Stefan Problem

Consider a plane layer of liquid PCM initially in equilibrium at T_m and having initial thickness L_0; it is in contact with the canister wall at $X = 0$, and with solid PCM at $X = L_0$. At time $t_0 = 0$, heat flux q is suddenly applied at $X = 0$, yielding the following boundary value problem:

$$\frac{1}{a}\frac{\partial T}{\partial t} = \frac{\partial^2 T}{\partial X^2} \tag{B1}$$

$$T(X, t_0) = T_m \tag{B2}$$

$$T[L(t), t] = T_m \tag{B3}$$

$$-k\left.\frac{\partial T}{\partial X}\right|_{X=0} = q \tag{B4}$$

$$-k\left.\frac{\partial T}{\partial X}\right|_{X=L(t)} = \rho H\frac{dL}{dt} \tag{B5}$$

$$L(0) = L_0 \tag{B6}$$

Here a = thermal diffusivity, and H = latent heat of fusion.

This is a penetration-type boundary-layer problem in which the "disturbance," q, propagates from $X = 0$ as the boundary-layer thickness

$$\delta(t) = \sqrt{6at} \tag{B7}$$

to reach the phase-change boundary in time t_1, where $\delta(t_1) = L_0$ (e.g., Arpachi and Larsen[13]):

$$t_1 = L_0^2/6a \tag{B8}$$

During this time interval, $0 \le t \le t_1$, the wall temperature increases as

$$T_w = T_m + q\delta(t)/2k = T_m + q\sqrt{(6at)}/2k \tag{B9}$$

with

$$T_{w1} = T_w(t_1) = T_m + qL_0/2k \tag{B10}$$

No changes occur at the phase-change boundary until $t > t_1$. It is noted, however, that for arbitrarily thin initial liquid layers [$\lim(L_0) \to 0$], both t_1 and $\delta(t)$ approach zero, so that there is *no* temperature increase in this limit. This is the case when the solid PCM initially contacts the canister wall.

Two time scales are evident in the system, [Eqs. (B1–B6)], the diffusion time $t_d = L_0^2/a$, and the phase-change time $t_p = \rho H L_0/q$, with $t_d \ll t_p$. This makes the system a classical singular perturbation problem in time, which may be solved by asymptotic expansions or multivariable methods[24,25]; in combination with the integral approximation,[13] this yields to lowest order the composite expansion

$$T_w = T_{w1} + \frac{q^2}{k\rho H}(t - t_1) + \frac{qL_0}{2k}\{1 - \exp[-3a(t - t_1)/L_0^2]\} \quad \text{(B11)}$$

It is seen in Eq. (B11) that there is a discontinuity in wall temperature as represented by the "inner-time" exponential. But, again, for $L_0 \to 0$, this singularity is removed and only the outer "quasisteady" solution remains

$$T_{w,\text{outer}} = T_m + (q^2/k\rho H)t \quad \text{(B12)}$$

It is noteworthy that the linear outer-time solution satisfies the initial condition $T_w(0) = T_m$, in contrast to the conventional temperature Stefan problem where the initial wall temperature at t_0^+ is not T_m.

Therefore, for the solid PCM initially contacting the canister wall, or for small initial liquid layers, there is no significant boundary-layer effect, or effect of the liquid specific heat, and the outer-time solution provides the whole solution to the problem. This conclusion is also reached when the initial temperature profile is different from constant at T_w.

Acknowledgment

This work was carried out under NASA Contract NAG3-1106, Lewis Research Center, Cleveland, Ohio.

References

[1]Labus, T. L., Secunde, R. R., and Lovely, R. G., "Solar Dynamic Power for Space Station Freedom," *Space Power*, Vol. 8, Nos. 1/2, 1989, pp. 97–114.

[2]Strumpf, H. J., and Coombs, M. G., "Solar Receiver Experiment for the Space Station Freedom Brayton Cycle," *Journal of Solar Energy Engineering*, Vol. 112, Feb. 1990, pp. 12–18.

[3]Namkoong, D., "Thermal Energy Storage Flight Experiments," *Proceedings of the ASME Solar Energy Conference*, San Diego, CA, April 2–5, 1989, pp. 19–24.

[4]Namkoong, D., "Flight Experiment of Thermal Energy Storage," *Proceedings of the 24th Intersociety Energy Conversion Engineering Conference*, Washington, DC, Aug. 6–11, 1989, pp. 953–957.

[5]Kerslake, T. W., and Ibrahim, M. B., "Analysis of Thermal Energy Storage Material with Change-of-Phase Volumetric Effects," *Proceedings of the ASME International Solar Energy Conference*, Miami, FL, April 1–4, 1990, pp. 315–325.

[6]Wichner, R. P., Solomon, A. D., Drake, J. B., and Williams, P. T., "Thermal Analysis of Heat Storage Canisters for a Solar Dynamic, Space Power System," *Proceedings of the ASME Solar Energy Conference*, Denver, CO, April 10–14, 1988, pp. 319–328.

[7]Williams, P. T., "Thermal Radiative Transport Through Lithium Fluoride for Temperatures Near the Melting Point," Oak Ridge Gaseous Diffusion Plant, Rept. K/CSD/TM-77, Oak Ridge, TN, 1988.

[8]Song, B., and Viskanta, R., "Deicing of Solids Using Radiant Heating," *Journal of Thermophysics and Heat Transfer*, Vol. 4, No. 3, 1990, pp. 311–317.

[9]Palik, E. D., and Hunter, W. R., "Lithium Fluoride (LiF)," *Handbook of Optical Constants of Solids*, Academic Press, New York, 1985, pp. 675–693.

[10]Yao, L. S., and Prusa, J., "Melting and Freezing," *Advances in Heat Transfer*, Vol. 19, Academic Press, New York, 1989, pp. 1–95.

[11]Burmeister, L. C., *Convective Het Transfer*, Wiley, New York, 1983, p. 169.

[12]Solomon, A., "A Note on the Stefan Number in Slab Melting and Solidification," *Letters Heat Mass Transfer*, Vol. 8, No. 3, 1981, pp. 229–235.

[13]Arpaci, V. S., and Larsen, P. S., *Convection Heat Transfer*, Prentice-Hall, Englewood Cliffs, NJ, 1984.

[14]Incropera, F. P., and DeWitt, D. P., *Introduction to Heat Transfer*, Wiley, New York, 1985, p. 402.

[15]Zhang, Z., and Bejan, A., "Melting in an Enclosure Heated at a Constant Rate," *International Journal of Heat and Mass Transfer*, Vol. 32, No. 6, 1989, pp. 1063–1076.

[16]Bayazitoglu, Y., and Lam T. T., "Marangoni Convection in Radiating Fluids," *Journal of Heat Transfer*, Vol. 109, Aug. 1987, pp. 717–721.

[17]Arnold, W., Gaug, J. R., and Chait, A., "Convection Phenomena in Low-Gravity Processing: The GTE GaAs Space Experiment," Aerospace Sciences Meeting, AIAA Paper 90-0409, Reno, NV, Jan. 8–11, 1990.

[18]Evans, G. W., II, Isaacson, E., and MacDonald, J. K. L., "Stefan-Like Problems," *Quarterly of Applied Mathematics*, Vol. 8, No. 3, 1950, pp. 312–319.

[19]Sparrow, E. M., and Cess, R. D., *Radiation Heat Transfer–Augmented Edition*, McGraw-Hill, New York, 1978.

[20]Seban, R. A., "The Emissivity of Transition Metals in the Infrared," *Journal of Heat Transfer*, Vol. 87, No. 2, 1965, pp. 173–176.

[21]Touloukian, Y. S., and DeWitt, D. P., "Thermal Radiative Properties," *Thermophysical Properties of Matter*, Vol. 7, edited by Y. S. Touloukian and C. Y. Ho, TPRC Data Series, IFI Plenum, New York, 1970.

[22]Siegel, R., and Howell, J. R., *Thermal Radiation Heat Transfer*, 2nd ed., Hemisphere, New York, 1981.

[23]Edwards, D. K., *Radiation Heat Transfer Notes*, Hemisphere, New York, 1981.

[24]Nayfeh, A. H., *Introduction to Perturbaton Techniques*, Wiley, New York, 1981.

[25]Smith, D. R., *Singular Perturbation Theory*, Cambridge Univ. Press, New York, 1985.